

Phase diagram and quench dynamics of a periodically driven Haldane model

Minxuan Ren(任民烜), Han Yang(杨焓), and Mingyuan Sun(孙明远)

Citation: Chin. Phys. B, 2024, 33 (**9**): 090309. DOI: 10.1088/1674-1056/ad4eb3
Journal homepage: http://cpb.iphy.ac.cn; http://iopscience.iop.org/cpb

What follows is a list of articles you may be interested in

Dynamical nonlinear excitations induced by interaction quench in a two-dimensional box-trapped Bose-Einstein condensate

Zhen-Xia Niu(牛真霞) and Chao Gao(高超)
Chin. Phys. B, 2024, 33 (**2**): 020314. DOI: 10.1088/1674-1056/ad1179

Effects of quantum quench on entanglement dynamics in antiferromagnetic Ising model

Yue Li(李玥), Panpan Fang(房盼盼), Zhe Wang(王哲), Panpan Zhang(张盼盼), Yuliang Xu(徐玉良), and Xiangmu Kong(孔祥木)
Chin. Phys. B, 2023, 32 (**10**): 100303. DOI: 10.1088/1674-1056/ace15c

Exact solution of slow quench dynamics and nonadiabatic characterization of topological phases

Rui Wu(邬睿), Panpan Fang(房盼攀), Chen Sun(孙辰), and Fuxiang Li(李福祥)
Chin. Phys. B, 2023, 32 (**8**): 080304. DOI: 10.1088/1674-1056/acd0a5

Quantum simulation of lattice gauge theories on superconducting circuits: Quantum phase transition and quench dynamics

Zi-Yong Ge(葛自勇), Rui-Zhen Huang(黄瑞珍), Zi-Yang Meng(孟子杨), and Heng Fan(范桁)
Chin. Phys. B, 2022, 31 (**2**): 020304. DOI: 10.1088/1674-1056/ac380e

Zitterbewegung of Dirac quasiparticles emerged in a Su-Schrieffer–Heeger lattice

Yue Hu(胡玥), Zheng-Xin Guo(郭政鑫), Ze-Ming Zhong(钟泽明), and Zhi Li(李志)
Chin. Phys. B, 2020, 29 (**11**): 110302. DOI: 10.1088/1674-1056/abb45b

---

Phase diagram and quench dynamics of a periodically driven Haldane model

Minxuan Ren(任民烜)†, Han Yang(杨焓), and Mingyuan Sun(孙明远)

School of Science, Beijing University of Posts and Telecommunications, Beijing 100876, *China*

(Received 14 March 2024; revised manuscript received 14 May 2024; accepted manuscript online 22 May 2024)

We investigate a periodically driven Haldane model subjected to a two-stage driving scheme in the form of a step function. By using the Floquet theory, we obtain the topological phase diagram of the system. We also find that anomalous Floquet topological phases exist in the system. Focusing on examining the quench dynamics among topological phases, we analyze the site distribution of the 0-mode and π-mode edge states in long-period evolution after a quench. The results demonstrate that, under certain conditions, the site distribution of the 0-mode can be confined at the edge even in long-period evolution. Additionally, both the 0-mode and π-mode can recover and become confined at the edge in long-period evolution when the post-quench parameters $\left(T, \frac{M_2}{M_1}\right)$ in the phase diagram cross away from the phase boundary $\frac{M_2}{M_1} = \frac{6\sqrt{3}t_2}{M_1} - 1$. Furthermore, we conclude that whether the edge state is confined at the edge in the long-period evolution after a quench depends on the similarity of the edge states before and after the quench. Our findings reveal some new characteristics of quench dynamics in a periodically driven system.

Keywords: Floquet system, Haldane model, quench dynamics, topological phase diagram

PACS: 03.65.Vf, 03.65.Ge **DOI:** 10.1088/1674-1056/ad4eb3

1. Introduction

Topological phases featuring gapless surfaces and edge modes have attracted increasing interest across various subfields of physics. One important research direction is the exploration of new topological phases through periodic driving, also known as Floquet systems.[1–6] Floquet systems offer a lot of intriguing phenomena, including anomalous topological phases in non-Hermitian systems,[7–11] Floquet topological phase transition,[12–16] and nonequilibrium Floquet steady states.[17–21]

In recent years, there has been a growing interest in studying topological phases and their characterization in periodically driven systems using cold atomic systems.[22–32] These studies have led to the discovery of various novel topological phases. Extensive investigations have been conducted to understand the topological properties of these novel topological phases, including the modified bulk–boundary correspondence (BBC),[5,33–36] band inversion surfaces (BISs) of Floquet bands,[37–40] and large-Chern-number topological phases.[41–46]

The Haldane model, which introduced the concept of topological insulators (TIs), has been extensively studied both theoretically and experimentally.[3,47–52] The dynamics of the Haldane model following a sudden quench within the topological phase have also been explored.[53–57] However, less is known about the dynamics of the periodically driven Haldane model under a quantum quench, where the dynamics are more complex than in the static Haldane model.

In this paper, we investigate a periodically driven Haldane model driven by a two-stage driving scheme in the form of a step function. Specifically, we examine the quench dynamics of this system and address key questions such as the topological properties of the periodically driven Haldane model, how the topological characteristics influence the dynamics of edge states, and what happens to the 0-mode and π-mode.

2. Floquet topological theory

We start discussions from a time-periodic driving system $\hat{H}(t) = \hat{H}(t+T)$ with period T. The Floquet eigenvalue equation gives (with $\hbar = 1$) $\hat{U}(T)|\psi(0)\rangle = \mathrm{e}^{-\mathrm{i}\varepsilon T}|\psi(0)\rangle$, where $\hat{U}(T) = \hat{\mathbb{T}}\exp\left[-\mathrm{i}\int_0^T \hat{H}(t)\,\mathrm{d}t\right]$ is the evolution operator with $\mathbb{T}$ being the time-ordering operator. ε are the quasienergies and $\psi(0)$ are the Floquet eigenstates.[59,60] Here, the quasienergies ε play the same role as the eigen-energy in a static system and lie in the Floquet bands $\left(-\frac{\pi}{T}, \frac{\pi}{T}\right]$. To relate the periodic evolution operator to the evolution of a static system, we define an effective Hamiltonian $\hat{H}_{\mathrm{F}}$: $\hat{H}_{\mathrm{F}} \equiv \frac{\mathrm{i}}{T}\ln\hat{U}(T)$. Thus, the topological properties of the time-periodic driving system can be investigated by the quasienergy spectrum of the Floquet system.

For each value of the momentum vector $\boldsymbol{k} = (k_x, k_y)$, a general static two-dimensional two-band Hamiltonian is

$$\mathcal{H}(\boldsymbol{k}) = \varepsilon(\boldsymbol{k})\boldsymbol{I}_{2\times 2} + \boldsymbol{h}(\boldsymbol{k})\cdot\boldsymbol{\sigma}, \tag{1}$$

where $\boldsymbol{\sigma}$ are the Pauli matrices, $\boldsymbol{I}_{2\times 2}$ is the identity matrix.

We establish a protocol of period $T = T_1 + T_2$, and the system Hamiltonian periodically quenches between two different

†Corresponding author. E-mail: renminxuanphy@bupt.edu.cn

© 2024 Chinese Physical Society and IOP Publishing Ltd

sets of values $\mathcal{H}_1$ and $\mathcal{H}_2$ within the respective time T_1 and T_2. Then, the effective Hamiltonian of this system is given by[45]

$$\begin{aligned}\mathcal{H}_F(\boldsymbol{k}) &\equiv \frac{\mathrm{i}}{T_1+T_2}\ln\left[\mathrm{e}^{-\mathrm{i}\mathcal{H}_2(\boldsymbol{k})T_2}\mathrm{e}^{-\mathrm{i}\mathcal{H}_1(\boldsymbol{k})T_1}\right]\\ &= \frac{\mathrm{i}}{T_1+T_2}\ln\left[\mathrm{e}^{-\mathrm{i}\boldsymbol{h}_2(\boldsymbol{k})\cdot\boldsymbol{\sigma}T_2}\mathrm{e}^{-\mathrm{i}\boldsymbol{h}_1(\boldsymbol{k})\cdot\boldsymbol{\sigma}T_1}\right], \quad (2)\end{aligned}$$

where $\mathcal{H}_{1,2}$ are expressed in terms of vectors $\boldsymbol{h}_{1,2}(\boldsymbol{k})$ according to Eq. (1). For this periodic quenching two-band system, the band touching of the quasienergy spectrum at $\varepsilon = 0, \pm\pi/T$ leads to topological phase transitions. The evolution operator reads $\hat{U}(T) = \mathrm{e}^{-\mathrm{i}\boldsymbol{h}_2\cdot\boldsymbol{\sigma}T_2}\mathrm{e}^{-\mathrm{i}\boldsymbol{h}_1\cdot\boldsymbol{\sigma}T_1}$. From the Euler form of Pauli matrix $\mathrm{e}^{-\mathrm{i}\boldsymbol{h}\cdot\boldsymbol{\sigma}t} = \cos(|\boldsymbol{h}|t) - \mathrm{i}\sin(|\boldsymbol{h}|t)\,\boldsymbol{h}\cdot\boldsymbol{\sigma}/|\boldsymbol{h}|$, we can obtain the effective Floquet Hamiltonian $\mathcal{H}_\mathrm{F} = \boldsymbol{h}_\mathrm{F}\cdot\boldsymbol{\sigma}$ with $\boldsymbol{h}_\mathrm{F} = -\arccos(\varepsilon_U)\,\boldsymbol{r}_U/(|\boldsymbol{r}_U|\cdot T)$ and

$$\begin{aligned}\varepsilon_U &= \cos|T_1\boldsymbol{h}_1|\cos|T_2\boldsymbol{h}_2| \\ &\quad - \frac{\boldsymbol{h}_1\cdot\boldsymbol{h}_2}{|\boldsymbol{h}_1|\cdot|\boldsymbol{h}_2|}\sin|T_1\boldsymbol{h}_1|\sin|T_2\boldsymbol{h}_2|, \quad (3)\\ \boldsymbol{r}_U &= \frac{\boldsymbol{h}_1\times\boldsymbol{h}_2}{|\boldsymbol{h}_1|\cdot|\boldsymbol{h}_2|}\sin|T_1\boldsymbol{h}_1|\sin|T_2\boldsymbol{h}_2| \\ &\quad - \frac{\boldsymbol{h}_1}{|\boldsymbol{h}_1|}\sin|T_1\boldsymbol{h}_1|\cos|T_2\boldsymbol{h}_2| \\ &\quad - \frac{\boldsymbol{h}_2}{|\boldsymbol{h}_2|}\sin|T_2\boldsymbol{h}_2|\cos|T_1\boldsymbol{h}_1|. \quad (4)\end{aligned}$$

We obtain the condition from Eq. (3), which states that the band touches and leads to topological phase transitions when[45]

$$\frac{\boldsymbol{h}_1\cdot\boldsymbol{h}_2}{|\boldsymbol{h}_1|\cdot|\boldsymbol{h}_2|} = \pm 1, \;\; T_1|\boldsymbol{h}_1| \pm T_2|\boldsymbol{h}_2| = m\pi, \quad (5)$$

with m being an even (odd) integer for $\varepsilon = 0$ $(\pm\pi/T)$.

The topological characteristics can be evaluated by the Floquet Chern number, which can be calculated (for the lower band) from[4]

$$C_\mathrm{F} = \frac{1}{4\pi}\int_\mathrm{FBZ}\frac{\boldsymbol{h}_\mathrm{F}}{|\boldsymbol{h}_\mathrm{F}|^3}\cdot\left(\partial_{k_x}\boldsymbol{h}_\mathrm{F}\times\partial_{k_y}\boldsymbol{h}_\mathrm{F}\right)\mathrm{d}^2\boldsymbol{k}. \quad (6)$$

However, the topological properties of the system cannot be fully described by calculating the Floquet Chern number alone, and we need to consider the winding number.[5] The winding number can be calculated as

$$\begin{aligned}&n_\mathrm{edge}(\varepsilon) = W_\varepsilon \\ &= \frac{1}{8\pi^2}\int\mathrm{d}t\,\mathrm{d}k_x\,\mathrm{d}k_y\,\mathrm{Tr}\left(U_\varepsilon^{-1}\partial_t U_\varepsilon\cdot\left[U_\varepsilon^{-1}\partial_{k_x}U_\varepsilon, U_\varepsilon^{-1}\partial_{k_y}U_\varepsilon\right]\right). \quad (7)\end{aligned}$$

Here W_ε is the winding number at a quasienergy ε lying within a Floquet gap, with the modified time-evolution operator U_ε being constructed as follows:

$$U_\varepsilon(\boldsymbol{k},t) = \begin{cases} U(\boldsymbol{k},2t), & 0\le t\le\frac{T}{2}, \\ V_\varepsilon(\boldsymbol{k},2T-2t), & \frac{T}{2}\le t\le T, \end{cases} \quad (8)$$

where $V_\varepsilon(\boldsymbol{k},t) = \mathrm{e}^{-\mathrm{i}\mathcal{H}_\mathrm{F}(\boldsymbol{k})t}$ with $\mathcal{H}_\mathrm{F}(\boldsymbol{k}) = \frac{\mathrm{i}}{T}\log U(\boldsymbol{k},T)$, and we choose the branch cut of the logarithm with

$$\begin{aligned}\log\mathrm{e}^{-\mathrm{i}\varepsilon T+\mathrm{i}0^-} &= -\mathrm{i}\cdot\varepsilon T, \\ \log\mathrm{e}^{-\mathrm{i}\varepsilon T+\mathrm{i}0^+} &= -\mathrm{i}\cdot\varepsilon T - 2\pi\mathrm{i}. \quad (9)\end{aligned}$$

3. Phase diagram of a periodically driven Haldane model

The Haldane model describes spinless fermions hopping on a 2D honeycomb both nearest and next nearest neighbor hopping parameters. The Hamiltonian is given by[47]

$$\begin{aligned}\hat{H} &= t_1\left(\sum_{\langle i,j\rangle}\hat{c}_i^\dagger\hat{c}_j + \mathrm{H.c.}\right) + t_2\left(\sum_{\langle\langle i,j\rangle\rangle}\mathrm{e}^{\mathrm{i}\phi_{ij}}\hat{c}_i^\dagger\hat{c}_j + \mathrm{H.c.}\right) \\ &\quad + M\sum_{i\in A}\hat{n}_i - M\sum_{i\in B}\hat{n}_i, \quad (10)\end{aligned}$$

where M is the staggered potential responsible for breaking the symmetry between the two sublattices of a honeycomb lattice, t_1 is the nearest-neighbor hopping, t_2 is the next-nearest-neighbor hopping, and A and B represent two different sublattices. $\hat{c}_i^\dagger$ $(\hat{c}_j)$ is the creation/annihilation operator at site i (j) , and $\hat{n}_i \equiv \hat{c}_i^\dagger\hat{c}_i$ is the corresponding number operator. The phase factor of next to nearest neighbor hopping, $\phi_{ij} = \pm\phi$, is positive for anticlockwise and negative for clockwise.

The Haldane model has been realized experimentally, and the dynamics induced by quantum quenches in the Haldane model have also been studied.[50,61–64] It is theoretically shown that the periodically quenched Haldane model can obtain a variety of topological phases, and this model has been realized experimentally in a nitrogen-vacancy (NV) system.[45,46] Inspired by the theoretical and experimental advances mentioned above, we consider an accessible two-step driving protocol of a periodically driven Haldane model:

$$M = \begin{cases} M_1, & t\in\left[NT, NT+\frac{T}{2}\right), \\ M_2, & t\in\left[NT+\frac{T}{2}, NT+T\right), \end{cases} \quad N\in\mathbb{N}. \quad (11)$$

Under the protocol of Eq. (11), the two instantaneous Hamiltonians can be written as (with the phase factor $\phi_{ij} = \pi/2$)

$$\begin{aligned}\boldsymbol{h}_1(\boldsymbol{k}) &= \Bigg(t_1\sum_{i=1,2,3}\cos(\boldsymbol{k}\cdot\boldsymbol{a}_i),\, t_1\sum_{i=1,2,3}\sin(\boldsymbol{k}\cdot\boldsymbol{a}_i), \\ &\quad M_1 - 2t_2\sum_{i=1,2,3}\sin(\boldsymbol{k}\cdot\boldsymbol{b}_i)\Bigg), \quad (12)\\ \boldsymbol{h}_2(\boldsymbol{k}) &= \Bigg(t_1\sum_{i=1,2,3}\cos(\boldsymbol{k}\cdot\boldsymbol{a}_i),\, t_1\sum_{i=1,2,3}\sin(\boldsymbol{k}\cdot\boldsymbol{a}_i), \\ &\quad M_2 - 2t_2\sum_{i=1,2,3}\sin(\boldsymbol{k}\cdot\boldsymbol{b}_i)\Bigg), \quad (13)\end{aligned}$$

where the primitive vectors $\boldsymbol{a}_1$, $\boldsymbol{a}_2$ and $\boldsymbol{a}_3$ are the units of the honeycomb lattice constant, $\boldsymbol{b}_1 = \boldsymbol{a}_2 - \boldsymbol{a}_3$, $\boldsymbol{b}_2 = \boldsymbol{a}_3 - \boldsymbol{a}_1$,

$\boldsymbol{b}_3 = \boldsymbol{a}_1 - \boldsymbol{a}_2$ are the three vectors connecting the nearest neighboring sites.

Through this drive scheme, we construct the periodically driven Haldane model and calculate the topological phase diagram in the T–$\frac{M_2}{M_1}$ plane (only the diagram for a small range of T and $\frac{M_2}{M_1}$ is plotted (see Appendix B)) as Fig. 2 shows. Different colors represent different topological phases. We find that the Floquet Chern number $C_{\rm F} = 0$ in the blue region of the phase diagram, but the existence of edge modes can be observed through the quasienergy spectrum of these phases (see Appendix A), which means that they are anomalous Floquet topological phases.[6] In fact, the Floquet Chern number can also be expressed as $C_{\rm F} = W_0 - W_\pi$.[5] So the Floquet Chern number of the anomalous Floquet topological phases can be obtained by $C_{\rm F} = W_0 - W_\pi = 1 - 1 = 0$. The phase boundaries of the phase diagram are determined by Eq. (5). For a two-band Floquet system, there are two edge states to consider between the two bands: 0-mode and π-mode.[5,6] In this phase diagram, we calculate the 0-mode phase boundary: $\frac{M_2}{M_1} = \frac{6\sqrt{3}t_2}{M_1} - 1$, $\frac{M_2}{M_1} = \frac{4\pi}{M_1}\cdot\left(\frac{1}{T}\right) - 1 - \frac{6\sqrt{3}t_2}{M_1}$ and the π-mode phase boundary: $\frac{M_2}{M_1} = \frac{2\pi}{M_1}\cdot\left(\frac{1}{T}\right) - 1 - \frac{6\sqrt{3}t_2}{M_1}$.

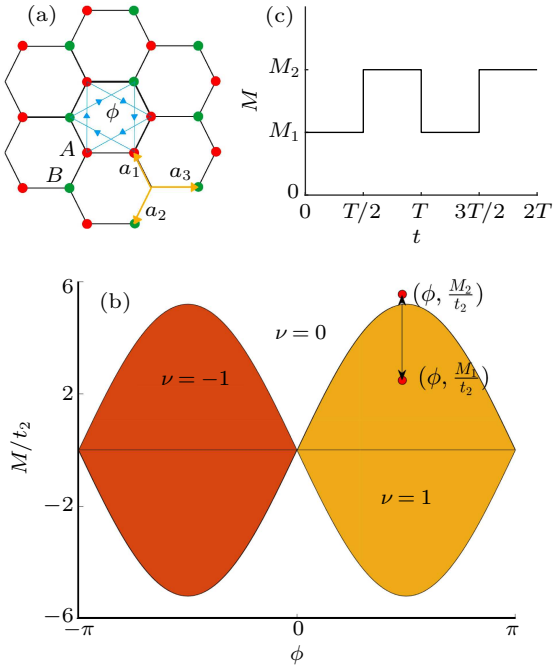


Fig. 1. (a) Two-dimensional honeycomb lattice with lattice primitive vectors $\boldsymbol{a}_1$, $\boldsymbol{a}_2$ and $\boldsymbol{a}_3$. Red and green circles represent the two sublattices A and B. (b) Phase diagram of the Haldane model, $\nu = \pm 1$ shows topological phase and $\nu = 0$ shows non-topological phase. (c) We consider a two-stage driving scheme in the form of a step function like (b) shows $\left(\phi, \frac{M_1}{t_2}\right) \leftrightarrow \left(\phi, \frac{M_2}{t_2}\right)$.

4. Quench dynamics of a periodically driven Haldane model

In this section, we study the quench dynamics of the periodic quenching Haldane model. We consider quantum quenches in different regions of the phase diagram, as illustrated by the arrow in Fig. 2. Here, we emphasize that for the topological phase diagrams with different parameters (M_1, t_1, t_2), our conclusions on quench dynamics are universal. To examine the robustness of the edge modes, we conducted a study on the evolution of these modes following a quantum quench. Since the edge modes exist in pairs, the right edge state's evolution after quenching is similar to that of the left edge state, so in this paper we only discuss the evolution of the left mode after the quantum quench. Initially, at time $t = 0$, we prepare the pre-quench state $\psi(0)$ with the pre-quench parameters $\left(T_0, \left(\frac{M_2}{M_1}\right)_0\right)$, which $\psi(0)$ served as quasi-static states. Subsequently, we abruptly change the post-quench parameters to $\left(T, \frac{M_2}{M_1}\right)$, resulting in the post-quench state $\psi(t)$ no longer remaining in quasi-static states after the quench. $\psi(t)$ can be expressed as

$$\psi(t) = \mathrm{e}^{-\mathrm{i}\mathcal{H}'_{\rm F} t}\psi(0), \tag{14}$$

where $\mathcal{H}'_{\rm F}$ represents the effective Floquet Hamiltonian of the system with the post-quench parameters $\left(T, \frac{M_2}{M_1}\right)$. Consequently, the site distribution of the edge state undergoes time evolution.

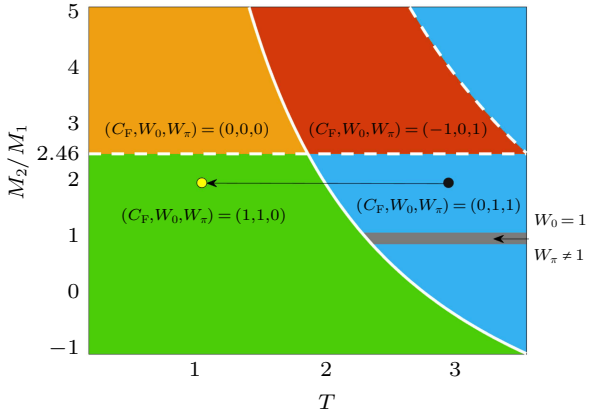


Fig. 2. Topological phase diagram of the periodically driven staggered potential M in the Haldane model. We label five different topological phases within the range of the parameters. The phases of grey region show band overlaps, which cause $W_\pi \neq 1$. In this phase diagram, we use the parameters $M_1 = 1/2, t_1 = 1/2, t_2 = 1/6, \phi = \pi/2$. Solid (dashed) lines correspond to the band-touching points at π-gap (0-gap). The diagram is only for a small range of T and M_2/M_1 as plotted. See Appendices A and B for more details about the topological phase diagram.

To investigate the impact of the quench, we focus on the site distribution of the edge states in long-period evolution. We observe that the distribution tends to stabilize after long-period evolution (see Appendix C). To facilitate our analysis, we uniformly select the time $t = 1000T$ to represent the long-period evolution of the system.

First, we consider the evolution of 0-mode and calculate the following cases (the following conclusions apply to the parameters within the scope of Fig. 2).

Case I $\frac{M_2}{M_1}$ remains invariant while T is changed. We investigate two distinct quenching regions, determined by the

phase boundary $\frac{M_2}{M_1} = \frac{6\sqrt{3}t_2}{M_1} - 1 = 2\sqrt{3} - 1$. When $\frac{M_2}{M_1} < 2\sqrt{3} - 1 \approx 2.46$, the 0-mode remains confined at the edge, roughly equivalent to the initial state distribution even in long-period evolution [as shown in Fig. 3(a)]. However, when $\frac{M_2}{M_1} > 2\sqrt{3} - 1$, the 0-mode is no longer highly confined at the left edge in long-period evolution [see Fig. 3(b)]. This discrepancy can be attributed to the different 0-mode states before and after the quench. Figures 3(c) and 3(d) illustrate the pre-quench edge states of the 0-mode. When $\frac{M_2}{M_1} < 2\sqrt{3} - 1$, the edge states of the 0-mode under these two parameters are approximately equivalent. This shows that in this region of the phase diagram, only adjusting the period T has little effect on the edge state of 0-mode, which is also the reason why 0-mode can be confined at the edge in long-period evolution when $\frac{M_2}{M_1}$ is invariant in the region of $\frac{M_2}{M_1} < 2\sqrt{3} - 1$. However, when $\frac{M_2}{M_1} > 2\sqrt{3} - 1$, the edge states of the 0-mode under the two parameters differ significantly, resulting in the observed loss of confinement at the left edge after a long period of evolution. In conclusion, quenching the 0-mode with $\frac{M_2}{M_1}$ kept constant and $\frac{M_2}{M_1} < 2\sqrt{3} - 1$ guides us to a universal method of confining the 0-mode at the edge in long-period evolution after a quench.

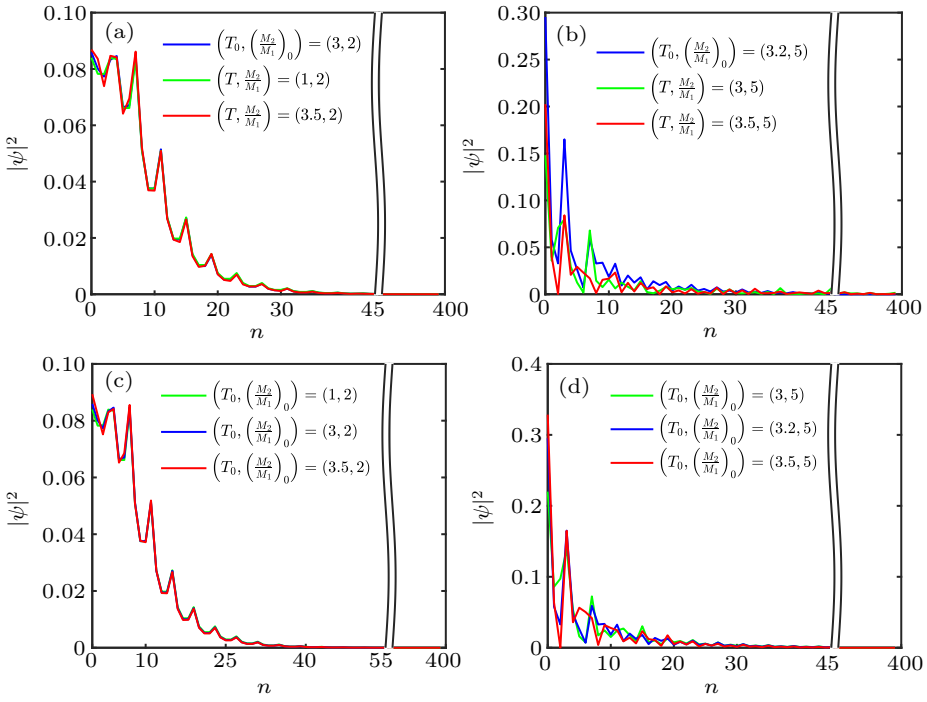


Fig. 3. Site distribution of 0-mode in long-period evolution $t = 1000T$ after a quench from the pre-quench parameters $\left(T_0, \left(\frac{M_2}{M_1}\right)_0\right)$ to post-quench parameters $\left(T, \frac{M_2}{M_1}\right)$. (a) $\left(T_0, \left(\frac{M_2}{M_1}\right)_0\right) = (3,2)$. (b) $\left(T_0, \left(\frac{M_2}{M_1}\right)_0\right) = (3.2,5)$. Meanwhile, (c) and (d) show the difference of the pre-quench 0-mode edge state. Here, n represents the n-th site number.

Case II Changing $\frac{M_2}{M_1}$ while keeping T invariant. First, we continue the selection of the pre-quench parameters $\left(T_0, \left(\frac{M_2}{M_1}\right)_0\right) = (3,2)$. Referring to Case I, we focus on the phase boundary $\frac{M_2}{M_1} = 2\sqrt{3} - 1$. When we change the pre-quench parameters to post-quench parameters $\left(T, \frac{M_2}{M_1}\right)$ that are close to the phase boundary $\frac{M_2}{M_1} = 2\sqrt{3} - 1$, we observe that the confinement of the 0-mode at the edge diminishes in long-period evolution. This trend becomes increasingly evident as the post-quench parameters $\left(T, \frac{M_2}{M_1}\right)$ approach the phase boundary [refer to Fig. 4(a)]. Since the post-quench parameters $\left(T, \frac{M_2}{M_1}\right)$ selected close to the phase boundary will cause the long-period evolution of 0-mode to no longer be confined at the edge, a natural question arises: can the 0-mode still be confined at the edge in long-period evolution when we select post-quench parameters far away from the phase boundary? Figure 4(b) indicates that this needs to be discussed in two situations: when the selected post-quench parameters $\left(T, \frac{M_2}{M_1}\right)$ cross the phase boundary $\frac{M_2}{M_1} = 2\sqrt{3} - 1$ relative to the initial state, the farther away from the phase boundary, the more the 0-mode with long-period evolution can be confined at the edge; however, when the post-quench parameters $\left(T, \frac{M_2}{M_1}\right)$ do not cross the phase boundary, the 0-mode may not tend to be confined at the edge in long-period evolution.

Next, we consider the different pre-quench states. We continue to change M_2/M_1 while keeping T invariant. We select the different pre-quench parameters in the topological phase regions (e), (f), and (g) in Fig. 2 as the initial state, and Figs. 4(c), 4(d), 4(e) show site distribution of the 0-mode in long-period evolution with different pre-quench parameters. As mentioned above, we can still observe that the 0-mode gradually recovers to be confined at the edge because

the post-quench parameters $\left(T, \frac{M_2}{M_1}\right)$ are far away from the phase boundary $\frac{M_2}{M_1} = 2\sqrt{3}-1$. Hence, we conclude that by sweeping the post-quench parameters $\frac{M_2}{M_1}$ while keeping T invariant and crossing different topological phases, the site distribution of the 0-mode undergoes distinct stages. Initially, the 0-mode is confined at the edge (in the initial state), but as the post-quench parameters begin to approach and cross the phase boundary $\frac{M_2}{M_1} = 2\sqrt{3}-1$, the confinement at the edge diminishes. However, we find that when the post-quench parameters $\left(T, \frac{M_2}{M_1}\right)$ are far away from the phase boundary, the confinement at the edge will be recovered. The underlying reasons behind the gradual recovery in the long-period evolution of the 0-mode, and its subsequent confinement at the edge after crossing the post-quench state away from the phase boundary, are worth investigating. We have discovered that the pre-quench edge state of the 0-mode tends to be less confined at the edge in the vicinity of the phase boundary $\frac{M_2}{M_1} = 2\sqrt{3}-1$ [see Fig. 4(f)]. However, since the post-quench parameters $\left(T, \frac{M_2}{M_1}\right)$ are further away from the phase boundary, the post-quench edge states gradually become highly confined. This phenomenon leads to a more analogous distribution of 0-mode edge states before and after a quench, enabling the 0-mode to recover and become confined at the edge in long-period evolution.

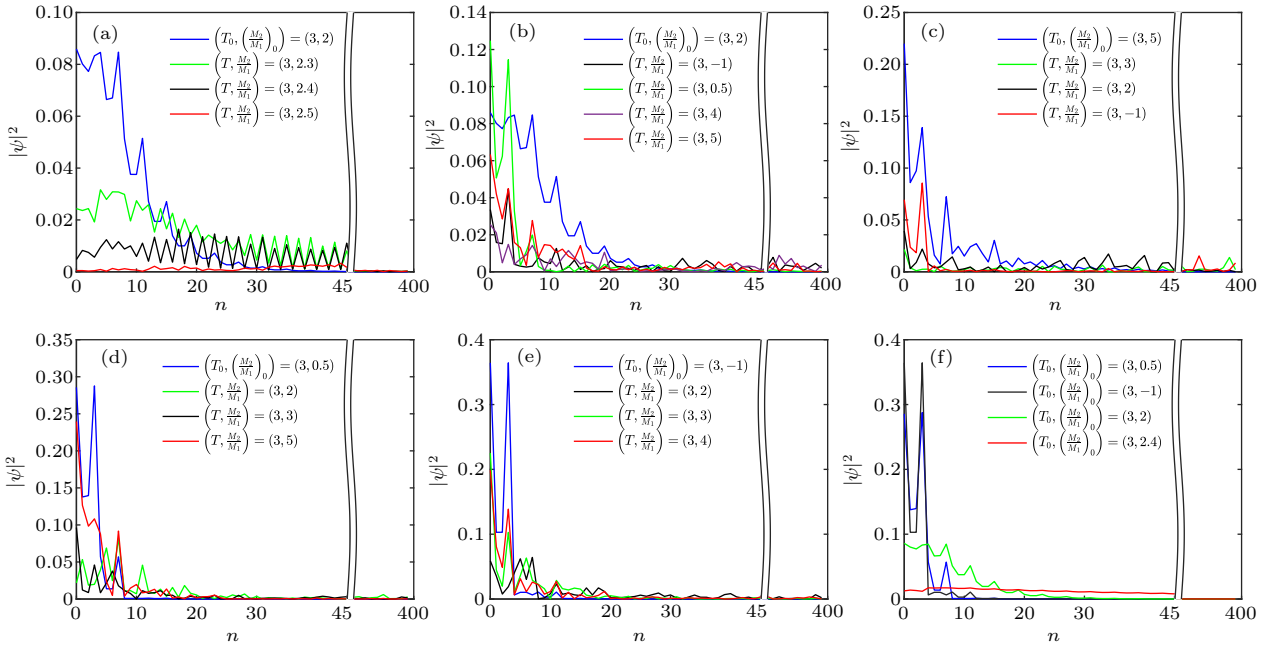


Fig. 4. Site distribution of 0-mode in long-period evolution $t = 1000T$ after a quench from the pre-quench parameters $\left(T_0, \left(\frac{M_2}{M_1}\right)_0\right)$ to post-quench parameters $\left(T, \frac{M_2}{M_1}\right)$. We select different pre-quench states located in different topological phases. (a), (b) $\left(T_0, \left(\frac{M_2}{M_1}\right)_0\right) = (3,2)$. (c) $\left(T_0, \left(\frac{M_2}{M_1}\right)_0\right) = (3,5)$. (d) $\left(T_0, \left(\frac{M_2}{M_1}\right)_0\right) = (3,0.5)$. (e) $\left(T_0, \left(\frac{M_2}{M_1}\right)_0\right) = (3,-1)$. Meanwhile, (f) shows pre-quench edge states of the 0-mode.

After studying the evolution of 0-mode, we shift our focus to the evolution of the π-mode. Upon observing the pre-quench states of the 0-mode and π-mode in Figs. 4 and 5, it becomes evident that the pre-quench state of the π-mode differs from that of the 0-mode under the same parameters $\left(T_0, \left(\frac{M_2}{M_1}\right)_0\right)$. This disparity will consequently lead to a distinct evolution of the π-mode after a quench compared to that of the 0-mode. Besides, the evolution of the π-mode cannot be universally confined at the edge after a long-period evolution, as observed in Case I. In our discussion of the 0-mode, we emphasized the phase boundary $\frac{M_2}{M_1} = 2\sqrt{3}-1$. Regarding the π-mode, our main concern still lies in this phase boundary. To further explore this, we continue to employ the method of varying $\frac{M_2}{M_1}$ while keeping T constant. Figures 5(a)–5(f) illustrate the evolution of the π-mode after a long-period evolution, starting from different initial states selected from various topological phase regions. Figures 5(a) and 5(c) indicate that when the post-quench parameters $\left(T, \frac{M_2}{M_1}\right)$ are close to the pre-quench parameters $\left(T_0, \left(\frac{M_2}{M_1}\right)_0\right)$, the π-mode remains confined at the edge in long-period evolution. As the post-quench parameters $\left(T, \frac{M_2}{M_1}\right)$ deviate from the pre-quench parameters, the confinement of the π-mode at the edge decreases. However, if the post-quench parameters $\left(T, \frac{M_2}{M_1}\right)$ cross away from the phase boundary $\frac{M_2}{M_1} = 2\sqrt{3}-1$, the π-mode recovers and becomes confined at the edge in long-period evolution. This behavior is similar to what we observed with the 0-mode, as illustrated in Figs. 5(b) and 5(d). Notably, even if we choose the post-quench parameters $\left(T, \frac{M_2}{M_1}\right)$ on the Haldane phase without the π-mode, the π-mode still exhibits strong confinement at the edge in long-period evolution after the quench.

Furthermore, we also explore the evolution of the π-mode using pre-quench parameters from different topologi-

cal phases and other quenching methods, such as changing T while keeping $\frac{M_2}{M_1}$ invariant. The results obtained are identical with the above discussions [see Figs. 5(e)–5(h)]. We have explained that the edge states of the 0-mode become less confined at the edge near the phase boundary $\frac{M_2}{M_1} = 2\sqrt{3}-1$. Although the pre-quench state of π-mode near the phase boundary $\frac{M_2}{M_1} = 2\sqrt{3}-1$ is still confined at the edge, it can be observed that the pre-quench state can be highly confined at the edge as the pre-quench parameters $\left(T_0, \left(\frac{M_2}{M_1}\right)_0\right)$ move away from the phase boundary, as shown in Fig. 5(h). In particular, we choose the 0-mode edge state for the pre-quench parameters on the Haldane phase, which allows us to compare the 0-mode edge state with the π-mode edge state. This is because the confinement of the edge state in long-period evolution is only related to the similarity of the edge states before and after the quench, and it is not necessary for the edge states before and after a quench to be all 0-mode or π-mode. This observation provides insight into why the π-mode with the post-quench parameters $\left(T, \frac{M_2}{M_1}\right)$ on the Haldane phase can be confined at the edge in long-period evolution. Therefore, we infer that the confinement of the edge states in long-period evolution depends on the similarity of edge states before and after a quench, and the existence of the 0-mode or π-mode does not have a decisive relationship with the robustness of edge states after a quench.

Another potential factor that affects the evolution of the edge state is the selection of the total site number n_{total}. In this case, we select the same parameters $\left(T_0, \left(\frac{M_2}{M_1}\right)_0\right) = (3,2) \to \left(T, \frac{M_2}{M_1}\right) = (3, 2.3)$ with different values of n_{total}. Taking logarithms of the distribution allows us to more intuitively investigate the differences in the distribution of different site numbers. Figure 6 illustrates that the distribution of post-quench evolution near the left edge for $n_{\text{total}} = 4000$, $n_{\text{total}} = 1000$, and $n_{\text{total}} = 400$ is essentially equivalent. However, the distribution for $n_{\text{total}} = 100$ differs from the other three parameters of n_{total} in the edge region, indicating that a relatively large total site number n_{total} is necessary to accurately describe the site distribution of the edge state in long-period evolution.

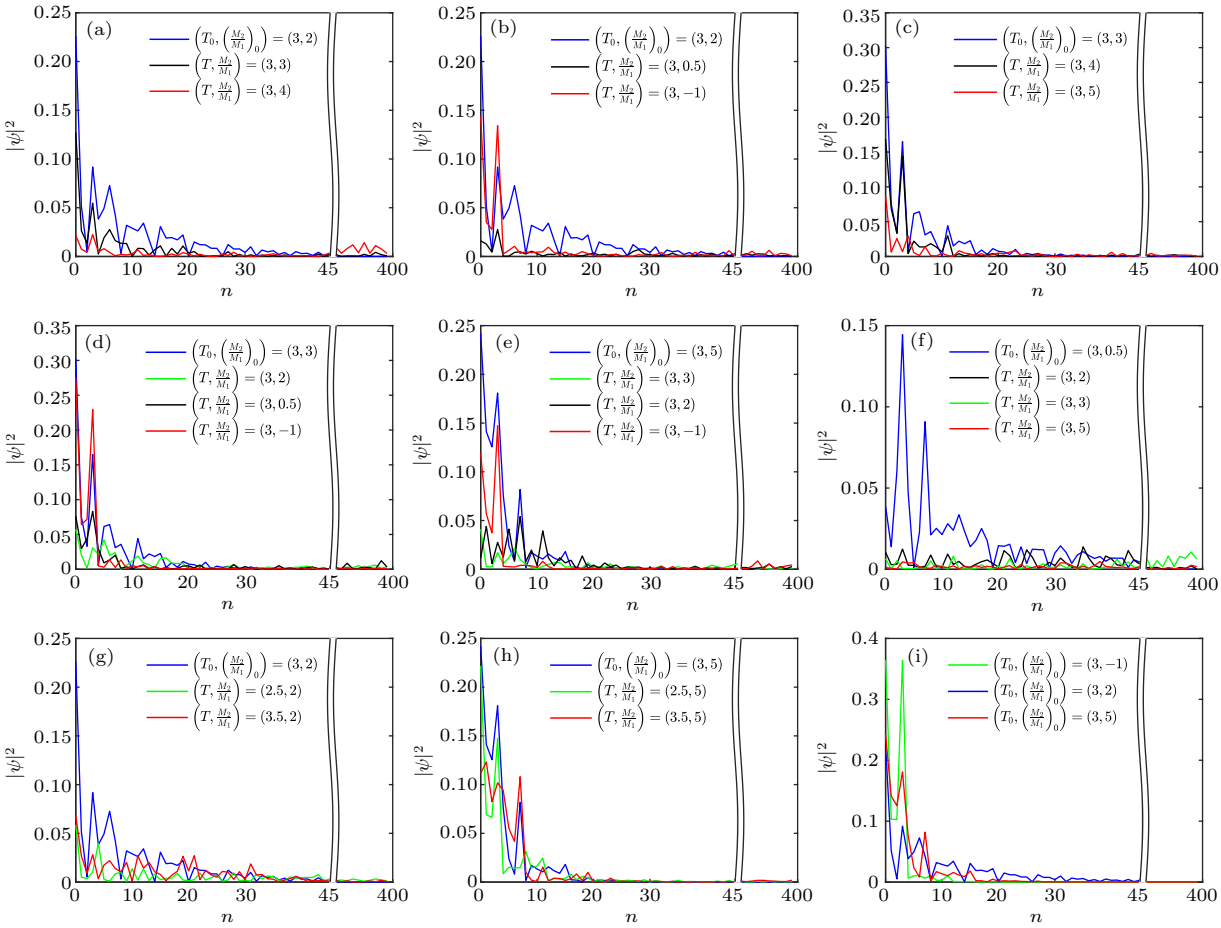


Fig. 5. Site distribution of π-mode in long-period evolution $t = 1000T$ from the pre-quench parameters $\left(T_0, \left(\frac{M_2}{M_1}\right)_0\right)$ to post-quench parameters $\left(T, \frac{M_2}{M_1}\right)$. We select different pre-quench states located in different topological phases. We use the method of changing $\frac{M_2}{M_1}$ while keeping T invariant in (a)–(f). (a), (b) $\left(T_0, \left(\frac{M_2}{M_1}\right)_0\right) = (3,2)$. (c), (d) $\left(T_0, \left(\frac{M_2}{M_1}\right)_0\right) = (3,3)$. (e) $\left(T_0, \left(\frac{M_2}{M_1}\right)_0\right) = (3,5)$. (f) $\left(T_0, \left(\frac{M_2}{M_1}\right)_0\right) = (3,0.5)$. (g), (h) We use the method of changing T while keeping $\frac{M_2}{M_1}$ invariant. Meanwhile, (i) shows pre-quench edge states. The edge states of $\left(T_0, \left(\frac{M_2}{M_1}\right)_0\right) = (3,2)$ and $\left(T_0, \left(\frac{M_2}{M_1}\right)_0\right) = (3,5)$ are the π-modes, the edge state of $\left(T_0, \left(\frac{M_2}{M_1}\right)_0\right) = (3,-1)$ is the 0-mode.

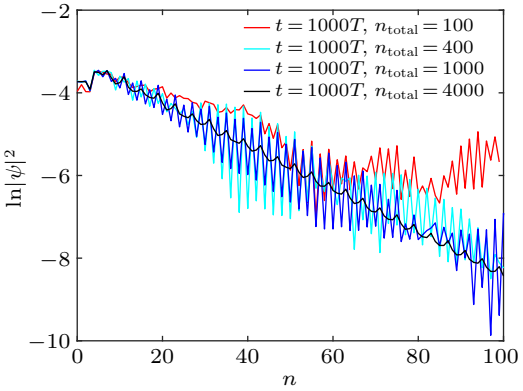


Fig. 6. Take the logarithm of the 0-mode distribution after a quench from $\left(T_0, \left(\frac{M_2}{M_1}\right)_0\right) = (3,2)$ to $\left(T, \left(\frac{M_2}{M_1}\right)\right) = (3,2.3)$ with the total site number $n_{\text{total}} = 4000$, $n_{\text{total}} = 1000$, $n_{\text{total}} = 400$ and $n_{\text{total}} = 100$.

5. Conclusion

In this study, we investigate the periodically driven Haldane model. We analyze the two-step driving scheme of the Haldane model and perform calculations on the quasienergy spectrum. Additionally, we construct a topological phase diagram by varying the parameter $\frac{M_2}{M_1}$ and period T. In this phase diagram, we observe the presence of anomalous Floquet topological phases characterized by the presence of edge modes, despite the Floquet Chern number $C_{\text{F}} = 0$. After examining the topological properties revealed by the phase diagram, we explore the dynamics that occur after a quench by adjusting the pre-quench parameters $\left(T_0, \left(\frac{M_2}{M_1}\right)_0\right)$ and post-quench parameters $\left(T, \frac{M_2}{M_1}\right)$.

Notably, we observe both differences and similarities in the dynamics of the edge states of the 0-mode and π-mode after a quantum quench. The pre-quench state of 0-mode and π-mode is different under the same parameters $\left(T_0, \left(\frac{M_2}{M_1}\right)_0\right)$, which will affect their evolution after the quench. In addition, the 0-mode can be effectively confined at the edge through long-period evolution, requiring changing T while maintaining $\frac{M_2}{M_1}$ and ensuring $\frac{M_2}{M_1} < \frac{6\sqrt{3}t_2}{M_1} - 1$. This phenomenon significantly distinguishes the 0-mode from the π-mode. We also find out that π-mode can still show strong confinement at the edge in long-period evolution when the post-quench parameters $\left(T, \frac{M_2}{M_1}\right)$ on the topological phase without the π-mode. The similarity of the 0-mode and π-mode is that when the post-quench states cross the phase boundary $\frac{M_2}{M_1} = \frac{6\sqrt{3}t_2}{M_1} - 1$, they can recover and become confined at the edge in long-period evolution.

Summarizing the evolution of 0-mode and π-mode, we emphasize that the confinement of the edge states in long-period evolution depends on the similarity of edge states before and after a quench. Additionally, the existence of the 0-mode or π-mode does not have a decisive relationship with the robustness of edge states after a quench. In future work, it will be meaningful to apply our research framework to more complex Floquet systems, such as periodically shaken square optical lattice systems[65–67] and periodic systems with continuous driving protocol,[68] and checking whether the edge modes are confined at the edge in long-period evolution after a quench.

Appendix A: Quasienergy spectrum and edge states in the periodically driven Haldane model

We calculate the energy spectrum of the effective Hamiltonian in the periodically driven Haldane model. The model is defined on a stripe terminated by an armchair edge in the y-direction and with periodic boundary conditions along x. Due to the periodicity along x, the Hamiltonian can be Fourier-transformed along this direction with $k_x \in [-\pi, \pi]$. Then, we calculated the effective Hamiltonian over one driving period according to Eq. (10) and the driving protocol of Eq. (11).

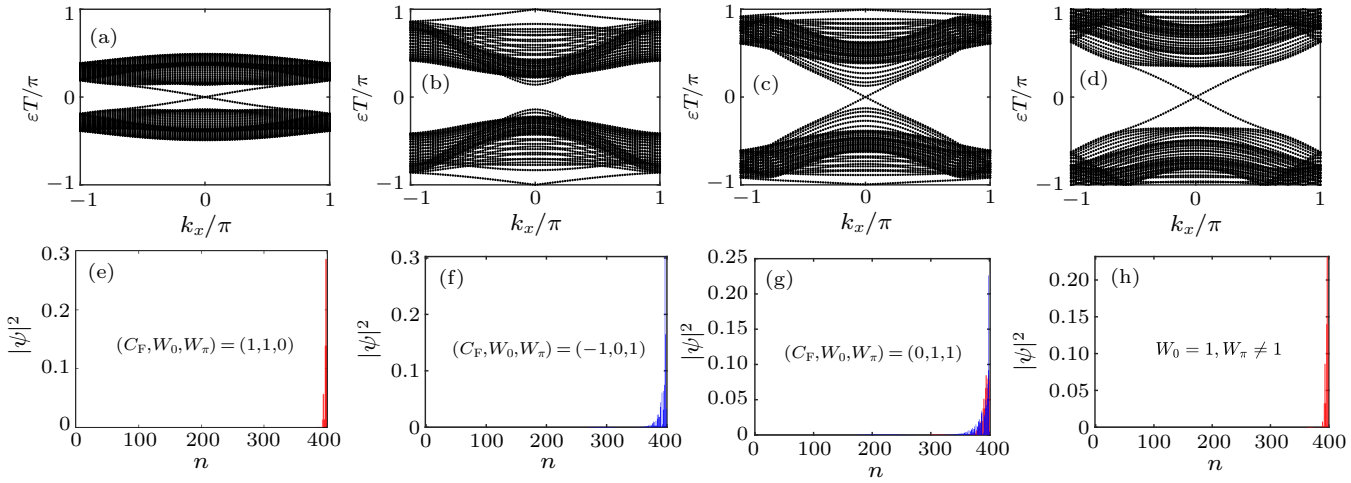


Fig. A1. (a)–(d) Quasienergy spectrum with $N = 100$ and (e)–(h) site distribution of the edge modes with positive group velocity $\partial_k \varepsilon$ for the periodically driven Haldane model. The parameters $\left(T, \frac{M_2}{M_1}\right)$ are $(1, 0.5)$ in panel (a), $(3,3)$ in panel (b), $(3,2)$ in panel (c), and $(3,1)$ in panel (d). There are two chiral edge modes, either traversing the zero quasienergy gap (marked with red) or traversing the π quasienergy gap (marked with blue). Here, we choose the edge state at $k_x = 0.005$.

In Fig. A1(a), we find a right-edge mode with positive group velocity that crosses the 0 quasienergy gap, and 0-mode contributes $(C_{\rm F}, W_0, W_\pi) = (1,1,0)$.[5,53,69] Similarly, Fig. A1(b) indicates that the π-mode right-edge state with positive group velocity contributes $(C_{\rm F}, W_0, W_\pi) = (-1,0,1)$; Fig. A1(c) shows two pairs of right-edge modes, with one pair traversing the 0 quasienergy gap and the other traversing the π quasienergy gap, and we obtain $(C_{\rm F}, W_0, W_\pi) = (0,1,1)$. This phenomenon reveals the existence of the anomalous Floquet topological (AFT) phase.[5,6]

Furthermore, we would like to mention that the topological phase of the region (d) of the topological phase diagram shown in Fig. 2 is not discussed in the main text. Figure A1(d) shows the quasienergy spectrum of this region. We can observe the band overlapping of the quasienergy spectrum at $\varepsilon = \pi/T$. The reason for this phenomenon is that we choose the parameter $M_2/M_1 \approx 1$ in region (d) of the phase diagram Fig. 2, which means that the staggered potential M does not change significantly in the period quenching. In this region, we cannot significantly change the topological properties of the system by changing the period T, so there is still only a 0-mode edge state in the calculated quasienergy spectrum. This phenomenon, where there is only the 0-mode edge state in the (d) region of the phase diagram, can also be reflected in Fig. A1(h).

Appendix B: Details about the phase diagram of the periodically driven Haldane model

We adapt the methodology outlined in the main text, maintaining a constant phase factor ϕ while varying the period T and the parameter M_2/M_1. This allows us to generate a new phase diagram. However, we change the value of M_1, causing the pre-quench state of the two-step driving protocol to be situated in the non-topological phase rather than the topological phase. Figure B1(a) visually demonstrates that the obtained phase diagram exhibits the fundamental characteristics outlined in the main text (see Fig. 2).

Furthermore, we employ an alternative approach wherein we keep the value of M constant while varying the period T and the phase factor ϕ. This alternative approach yields a novel topological phase diagram, as shown in Fig. B1(b). It is worth noting that a significant deviation arises because we cannot obtain the π-mode edge states using this approach given that Eq. (1) does not satisfy the necessary conditions.

Additionally, we choose a smaller period T in the phase diagram. When we choose a larger T, the topological properties of the system become more complicated, as shown in Figs. B1(c) and B1(d). For a large T, the quasienergy spectrum of the system will have band overlap at $\varepsilon = 0$ and $\varepsilon = \pi/T$. It is difficult to determine the topological properties of the quasienergy spectrum in the 0-mode and π-mode. Therefore, our phase diagram in this paper chooses the period $T < 4$.

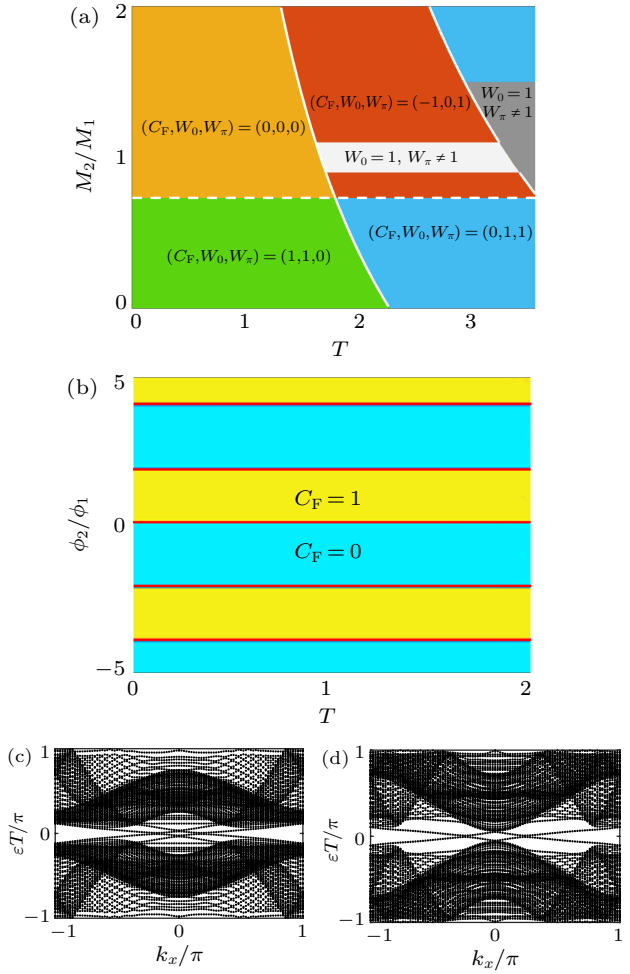


Fig. B1. (a) Topological phase diagram of the periodically driven staggered potential M in the Haldane model. In this topological phase diagram, we use the parameters: $\phi = \pi/2$, $M_1 = 1$, $t_1 = 1/2$, $t_2 = 1/6$. The phases of grey region and white region show band overlaps, which cause $W_\pi \neq 1$. (b) Topological phase diagram of the periodically driven phase factor ϕ in the Haldane model. This phase diagram we use the parameters: $\phi_1 = \pi/2$, $M = 1/2$, $t_1 = 1$, $t_2 = 1/6$. Quasienergy spectrum with the parameters $\left(T, \frac{M_2}{M_1}\right)$ are $(8,3)$ in panel (c) and $(10,3)$ in panel (d).

Appendix C: Long-period evolution in the periodically driven Haldane model

As mentioned in the main text, when we quench from the pre-quench parameters $\left(T_0, \left(\frac{M_2}{M_1}\right)_0\right)$ to the post-quench parameters $\left(T, \left(\frac{M_2}{M_1}\right)\right)$, the site distribution of the system will no longer remain in a quasi-static state. In this appendix, we discuss the details of the system evolution. As illustrated in Fig. C1, it is evident that the site distribution of edge states undergoes significant changes when the evolution time is short, such as $t = 20T$ or $t = 50T$, until it eventually converges to an edge distribution after a long period of evolution. We can observe that within the time range of $t = 0$ to $t = 50T$, the crest of the distribution moves between the position numbers. However, after $t > 200T$, the crest of the distribution tends to

stabilize. Consequently, we select the long period $t = 1000T$, in the main text to ensure the stability of the site distribution.

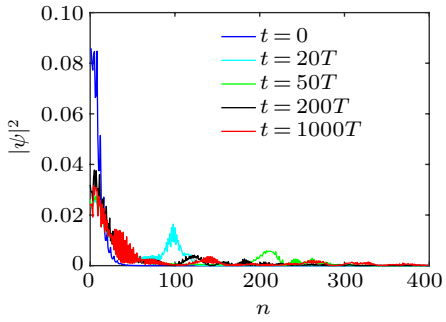


Fig. C1. Evolution of 0-mode site distribution after a quantum quench from $\left(T_0, \left(\frac{M_2}{M_1}\right)_0\right) = (3, 2)$ to $\left(T, \left(\frac{M_2}{M_1}\right)\right) = (3, 2.3)$.

Acknowledgements

We thank Ping Fang, Jieyun Yan, and Yueheng Lan for inspiring discussions. The project was supported by the National Natural Science Foundation of China (Grant No. 12004049).

References

[1] Thouless D J, Kohmoto M, Nightingale M P and Nijs M den 1982 *Phys. Rev. Lett.* **49** 405
[2] Wen X G 1990 *Int. J. Mod. Phys. B* **04** 239
[3] Hasan M Z and Kane C L 2010 *Rev. Mod. Phys.* **82** 3045
[4] Qi X L and Zhang S C 2011 *Rev. Mod. Phys.* **83** 1057
[5] Rudner M S, Lindner N H, Berg E and Levin M 2013 *Phys. Rev. X* **3** 031005
[6] Rudner M S and Lindner N H 2020 *Nat. Rev. Phys.* **2** 229
[7] Lee T E 2015 *Phys. Rev. Lett.* **116** 133903
[8] Yao S and Wang Z 2018 *Phys. Rev. Lett.* **121** 086803
[9] Xu Q Y, Liu F, Chen C Z and Xu D H 2020 *Phys. Rev. B* **105** 075411
[10] Zhou L and Gong J 2018 *Phys. Rev. B* **98** 205417
[11] Wu H and An J H 2020 *Phys. Rev. B* **102** 041119
[12] Kitagawa T, Berg E, Rudner M and Demler E 2010 *Phys. Rev. B* **82** 235114
[13] Else D V and Nayak C 2016 *Phys. Rev. B* **93** 201103
[14] Zhou L, Wang H, Ho D Y H and Gong J 2014 *Eur. Phys. J. B* **87** 204
[15] Zhou L and Du Q 2021 *J. Phys.: Condens. Matter* **33** 345403
[16] Luan L N, Zhang M Y, Wang L C 2023 *Chin. Phys. B* **32** 090302
[17] Bukov M, Gopalakrishnan S, Knap M and Demler E 2015 *Phys. Rev. Lett.* **115** 205301
[18] Seetharam K I, Bardyn C E, Lindner N H, Rudner M S and Refael J 2019 *Phys. Rev. B* **99** 014307
[19] Ikeda T N and Sato M 2020 *Sci. Adv.* **6** 27
[20] Cheng Z and Potter A C 2022 *Phys. Rev. B* **106** L220307
[21] Fazzini S, Chudzinski P, Dauer C, Schneider I and Eggert S 2021 *Phys. Rev. Lett.* **126** 243401
[22] Eckardt A 2015 *Rev. Mod. Phys.* **89** 011004
[23] Price H M, Ozawa T and Goldman N 2017 *Phys. Rev. A* **95** 023607
[24] Lin Y J, Jiménez-García K and Spielman I B 2011 *Nature* **471** 83
[25] Huang L, Meng Z, Wang P, Peng P, Zhang S L, Chen L, Li D, Zhou Q and Zhang J 2016 *Nat. Phys.* **12** 540
[26] Wu Z, Zhang L, Sun W, Xu X T, Wang B Z, Ji S C, Deng Y, Chen S, Liu X J and Pan J W 2016 *Science* **354** 6308
[27] Chen H R, Lin K Y, Chen P K, Chiu N C, Wang J B, Huang P, Yip S K, Kawaguchi Y and Lin Y J 2018 *Phys. Rev. Lett.* **121** 113204
[28] Luo X W, Zhou X, Li C F, Xu J S, Guo G C and Zhou Z W 2015 *Nat. Commun.* **6** 7704
[29] Zhang X, Jiang W, Deng J, Wang K, Chen J, Zhang P, Ren W, Dong H, Xu S, Gao Y, Jin J, Zhu X, Guo Q, Li H, Song C, Gorshkov A V, Iadecola T, Liu F, Gong Z X, Wang Z, Deng D L and Wang H 2022 *Nature* **607** 468
[30] Jünemann J, Piga A, Ran S J, Lewenstein M, Rizzi M and Bermudez A 2016 *Phys. Rev. X* **7** 031057
[31] Potirniche I D, Potter A C, Schleier-Smith M, Vishwanath A and Yao N Y 2017 *Phys. Rev. Lett.* **119** 123601
[32] Liu X J, Law K T, Ng T K and Lee Patrick A 2013 *Phys. Rev. Lett.* **111** 120402
[33] Peng Y G, Qin C Z, Zhao D G, Shen Y X, Xu X Y, Bao M, Jia H and Zhu X F 2016 *Nat. Commun.* **7** 13368
[34] Mukherjee S, Spracklen A, Valiente M, Andersson E, Öhberg P, Goldman N and Thomson R R 2017 *Nat. Commun.* **8** 13918
[35] Maczewsky L J, Zeuner J M, Nolte S and Szameit A 2017 *Nat. Commun.* **8** 13756
[36] Wintersperger K, Braun C, Ünal F N, Eckardt A, Liberto D M, Goldman N, Block I and Aidelsburger M 2020 *Nat. Phys.* **16** 1058
[37] Zhang L, Zhang L, Niu S and Liu X J 2018 *Sci. Bull.* **63** 1385
[38] Zhang L, Zhang L and Liu X J 2020 *Phys. Rev. Lett.* **125** 183001
[39] Zhang J Y, Yi C R, Zhang L, Jiao R H, Shi Y K, Yuan H, Zhang W, Liu X J, Chen S and Pan J W 2023 *Phys. Rev. Lett.* **130** 043201
[40] Zhang L and Liu X J 2022 *PRX Quantum* **3** 040312
[41] Barkeshli M and Qi X L 2012 *Phys. Rev. X* **2** 031013
[42] Wang Y F, Yao H and Gong C D 2012 *Phys. Rev. B* **86** 201101
[43] Wang J, Lian B, Zhang H, Xu Y and Zhang S C 2013 *Phys. Rev. Lett* **111** 136801
[44] Skirlo S A, Lu L, Igarashi Y, Yan Q, Joannopoulos J and Soljai M 2015 *Phys. Rev. Lett* **115** 253901
[45] Xiong T S, Gong J and An J H 2016 *Phys. Rev. B* **93** 184306
[46] Yang K, Xu S, Zhou L, Zhao Z, Xie T, Ding Z, Ma W, Gong J, Shi F and Du J 2022 *Phys. Rev. B* **106** 184106
[47] Haldane F D M 1988 *Phys. Rev. Lett* **61** 2015
[48] Wright A R 2013 *Sci. Rep.* **3** 2736
[49] Garrity K F and Vanderbilt D 2014 *Phys. Rev. B* **90** 121103
[50] Jotzu G, Messer M, Desbuquois R, Lebrat M, Uehlinger T, Greif D and Esslinger T 2014 *Nature* **515** 237
[51] Ding Y, Peng Y, Zhu Y, Fan X, Yang J, Liang B, Zhu X, Wan X and Cheng J 2017 *Phys. Rev. Lett* **122** 014302
[52] Wang C, Zhang P, Chen X, Yu J and Zhai H 2017 *Phys. Rev. Lett* **118** 185701
[53] Yu J 2017 *Phys. Rev. A* **96** 023601
[54] Caio M D, Cooper N R and Bhaseen M J 2015 *Phys. Rev. Lett* **115** 236403
[55] Mardanya S, Bhattacharya U, Agarwal A and Dutta A 2018 *Phys. Rev. B* **97** 115443
[56] Liou S F and Yang K 2018 *Phys. Rev. B* **97** 235144
[57] Ji H X, Mo L H and Wan X 2022 *Chin. Phys. Lett.* **39** 030301
[58] Mo L H, Zhang Q L and Wan X 2020 *Chin. Phys. Lett.* **37** 060301
[59] Sambe H 1973 *Phys. Rev. A* **7** 2203
[60] Chen C, An J H and Luo H G 2015 *Phys. Rev. A* **91** 052122
[61] Mitra S, Jiménez-Galán Á, Aulich M, Neuhaus M, Silva R E F, Pervak V, Kling M F and Biswas S 2024 *Nature* **62** 752
[62] Zhao W, Kang K, Zhang Y, Knüppel P, Tao Z, Li L, Tschirhart C L, Redekop E, Watanabe K, Taniguchi T, Young A F, Shan J and Mak K F 2024 *Nat. Phys.* **20** 275
[63] Tarnowski M, Ünal F N, Fläschner N, Rem B S, Eckardt A, Sengstock K and Weitenberg C 2019 *Nat. Commun.* **10** 1728
[64] Fläschner N and Vogel D, Tarnowski M, Rem B S, Lühmann D-S, Heyl M, Budich J C, Mathey L, Sengstock K and Weitenberg C 2018 *Nat. Phys.* **14** 265
[65] Miao J, Liu B and Zheng W 2015 *Phys. Rev. B* **91** 033404
[66] Keleş A, Zhao E and Liu W V 2017 *Phys. Rev. A* **95** 063619
[67] Chen H and Liu W V 2021 *Phys. Rev. A* **104** 013308
[68] Das D, Ghosh R and Sengupta K 2021 *J. High Energ. Phys.* **2021** 1-39
[69] Perez-Piskunow P M, Usaj G, Balseiro C A and Foa Torres L E F 2014 *Phys. Rev. B* **89** 121401